Modelling of the Dielectric Properties of Biological Tissues within the Histology Region

Emily Porter, Alessandra La Gioia, Adam Santorelli, and Martin O'Halloran
Translational Medical Device Laboratory, Electrical and Electronic Engineering,
2nd Floor Lambe Institute of Translational Research, National University of Ireland Galway
Galway, Ireland

Abstract— **The dielectric properties of biological tissues characterize the interaction of electromagnetic fields with the human body. As such, accurate knowledge of these properties is vital to the design and development of electromagnetic medical technologies. Despite their importance, the reported dielectric properties of key tissues have been inconsistent across studies. The natural heterogeneity of tissue has been identified as a contributing factor to these inconsistencies. In order to attribute dielectric properties to heterogeneous tissues, histological analysis is conducted to determine which tissue types contribute to the dielectric measurement. However, the Histology Region, i.e., the volume of the tissue sample that undergoes histological analysis, and the region corresponding to the dielectric measurement, has not been well-defined. Thus, instead of reducing uncertainties, more questions have been raised about the accuracy of data: if the Histology Region is not identified correctly, then the corresponding dielectric measurement does not represent the actual tissues involved. In this work, we examine the longitudinal extent of the Histology Region (i.e., the histology depth) for various heterogeneous samples composed of phantoms and biological tissues. This study highlights the fact that the relationship between the volume of tissue in a sample and the contribution of that tissue to the measured dielectric properties is not linear. Assuming that this relationship is linear may be a significant source of error in dielectric data. Further, we model, for the first time, the nonlinear relationship between the contribution of individual tissues to the dielectric measurement and the volume that each tissue occupies within the bulk sample. This work enables prediction of the permittivity of a sample with longitudinal heterogeneities, given knowledge of the constituent tissues of the sample, and provides the basis for modelling of all types of heterogeneities. These results will contribute to the minimization of uncertainties in the dielectric measurement of heterogeneous tissues.**

Index Terms— **Biological materials, dielectric measurement, open-ended coaxial probe, tissue properties.**

I. Introduction

THE dielectric properties dictate how electromagnetic energy is transmitted, absorbed, and reflected in the presence of biological tissues [1]. These properties, namely, the relative permittivity (ε_r) and the conductivity (σ), are inherent characteristics of all tissues. Knowledge of the dielectric properties is of vital importance for dosimetry studies, optimisation of wireless telecommunication devices, and for the design and application of novel electromagnetic (EM) medical devices [2]-[8].

The dielectric properties of tissues are typically measured using an open-ended coaxial probe placed in contact with the tissue of interest [9]-[12]. The probe is connected to a vector network analyzer, allowing the reflection coefficient, and thus the complex permittivity, to be recorded. Despite the apparent simplicity of the dielectric measurement process, historical reports have produced dielectric studies with conflicting results, most notably for highly heterogeneous tissues such as the breast [9]-[14]. These inconsistencies are mainly attributed to the fact that the coaxial probe is designed to measure homogeneous materials [15], and there is no standard procedure for measuring or interpreting the dielectric data for heterogeneous tissues. These inconsistencies present a serious problem for medical device researchers, as the true dielectric properties are unclear and therefore provide an unsatisfactory foundation for medical device design.

In order to attribute dielectric properties to heterogeneous tissues, researchers may conduct histological analysis [9]-[11]. Histological analysis provides information on what tissue types are present in a sample, and in what distribution or layout. This information can then be related to the dielectric properties. In order to perform histological

Manuscript received on March 8, 2017.

analysis, it is necessary to identify a region of the sample, the 'Histology Region', which will undergo the histological analysis, and to which the dielectric measurement corresponds. This region should encompass the volume of tissues which contribute to the dielectric measurement. Errors may be introduced into dielectric measurements of heterogeneous tissues when histology is not conducted (therefore it may not be clear which tissue or tissues contributed to the measurement), or when the region that undergoes histology is not accurately defined. In these situations, the dielectric data may not be correctly attributed to the tissues that resulted in the dielectric measurement.

The significance of the Histology Region is depicted in Figure 1. This image is a stained 2-D slice of a heterogeneous tissue sample, with different tissues types clearly visible by their different colours, sizes, and shapes. This image shows histology of a salivary gland sample, with carcinoma present. However, the figure should be taken as an illustrative example that applies to all heterogeneous tissues.

As marked on Figure 1, the Histology Region is a cylindrical volume, comprised of the histology radius, r_h, in the radial direction from the probe tip, and the histology depth, d_h, in the longitudinal direction from the probe tip. As can be seen from Figure 1, if r_h or d_h are incorrect, then the Histology Region either includes tissues which did not contribute to the dielectric measurement, or does not include all of the tissues which did contribute. In either case, the dielectric data is not correctly matched with the tissues that contributed to that dielectric measurement. For example, if the tissue within the Histology Region is composed of 75% adipose tissue and 25% glandular tissue, then the interpretation of the dielectric properties must reflect that.

However, the process of attributing dielectric properties to heterogeneous tissues is not straightforward. Recent studies [16], [17] suggest that the tissue closest to the dielectric measurement location (i.e., at the probe tip) contributes with disproportional dominance to the measured dielectric properties. This effect must be taken into consideration in order to have accurate interpretation of dielectric measurements of heterogeneous tissue samples.

In this work, we aim to provide a step towards achieving the goal of accurate correspondence between heterogeneous histology and dielectric measurements. In particular, we use samples of different combinations of phantoms and biological tissues, measure the histology depth, then calculate the weight of each tissues' contribution to the measured dielectric properties. We also calculate the volume occupied by each tissue, and compare this to the weight of contribution to the measured dielectric property. We find that this relationship is nonlinear, and model it using a logistic function, enabling correspondence between the tissue composition and the dielectric properties. Thereby, we enable modelling of the effect of longitudinal heterogeneities on the dielectric properties measured with an open-ended coaxial probe for the first time. This work provides the foundation for future studies to design a protocol for corresponding histology to dielectric measurements.

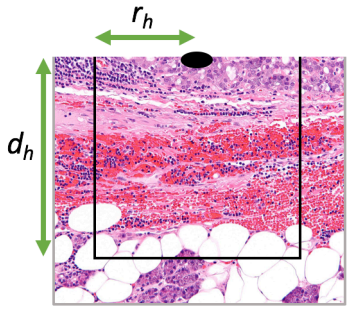

Figure 1. A histological slice from a heterogeneous tissue sample of acinic cell carcinoma (slice from [18]). The black oval indicates the dielectric probe position on the surface of the sample; the black outline indicates the Histology Region. The Histology Region is delimited by the histology depth (d_h) in the longitudinal direction and the histology radius (r_h) in the radial direction from the probe tip.

The paper is organized as follows: In Section II, the dielectric measurement set-up is introduced and the phantom and tissue samples are described. Then, the histology depths are determined for each measurement scenario. In Section III, the calculations for the contribution of each tissue to the dielectric properties are presented, along with the equation for obtaining the volume occupied by each tissue within the bulk sample. Next, in Section IV, the dielectric measurement data is presented along with the weights of each tissue's contribution to the dielectric data and the volume occupied by each tissue. In Section V, a model is introduced that enables correspondence between the contribution to the dielectric data and the tissue volume. Finally, in Section VI, the model application is discussed, along with an interpretation of the results. The paper concludes in Section VII.

II. Materials and Measurements

This section details the dielectric measurement set-up, the materials and tissues that are used in measurements, and the Histology Region.

A. Dielectric Measurement Set-up

Dielectric measurements were performed using the Keysight slim form probe (diameter 2.2 mm) connected to the Keysight E5063A network analyser. This probe was selected as its small diameter makes it optimal for measuring small tissue samples, and it is commonly used in the literature for this purpose [11], [12], [19], [20]. The probe was calibrated using the standard three-term calibration procedure.

The uncertainty of the measurement system was characterised after calibration by performing repeated measurements on a standard material of known dielectric properties (0.1 M NaCl). Using this data, the total combined uncertainty (TCU) [21] was calculated for both the relative permittivity and the conductivity. The TCU is calculated as the square root of the sum of squared distinct uncertainties, and includes Type A (repeatability) and Type B (accuracy) uncertainties related to the measurement set-up. The TCU was found to be 2.1 for relative permittivity and 3.4 for

conductivity. These values give the measurement uncertainty of the system. Specifically, the breakdown in uncertainty is: repeatability within 2.1% and 2.3%, and accuracy within 0.26% and 4.2%, for ε_r and σ, respectively. As the relative permittivity measurement is less affected by uncertainty, calculations for histology depth are based only on this parameter.

Measurements were recorded with 101 linearly spaced frequency points over 300 MHz – 8.5 GHz. This bandwidth was selected as it encompasses the frequencies of interest in many microwave medical applications. For example, it includes most microwave imaging systems, with frequencies spanning 1.3 GHz to 8 GHz [2], [4], [22]-[25]. It also encompasses general ablation systems (2.45 GHz, [7], [20]) and proposed breast hyperthermia (4.2-4.5 GHz, [6]). Since the breast is a highly heterogeneous organ that is commonly investigated, accurate knowledge of the Histology Region is particularly relevant.

In order to examine heterogeneous tissue structures, a measurement tank was developed based on the one in [17]. Within the tank, a solid material is placed on the bottom, surrounded by a liquid. The probe is inserted into the tank and immersed in the liquid. The probe is attached to a micrometer caliper which enables fine vertical movement. A diagram of this set-up is shown in Figure 2. With this set-up, tissue samples that are heterogeneous in the longitudinal (depth) direction are generated by varying t_1, i.e., the thickness of Tissue 1 (the liquid), which is also equal to the distance between the probe tip and the surface of Tissue 2 (the solid). In other words, each unique t_1 defines a unique heterogeneous sample containing various proportions of Tissue 1 and Tissue 2.

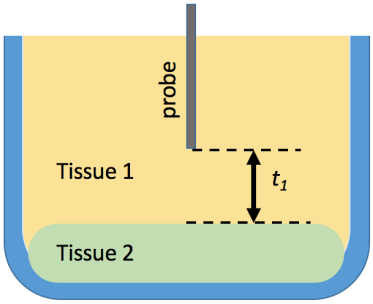

Figure 2. Schematic diagram of the dielectric measurement set-up. Tissue 2 (green) is fixed to the bottom of a tank, and the remainder of the tank is filled with liquid Tissue 1 (yellow). The probe (grey) is positioned within the tank, and can be moved vertically, thus varying the thickness of Tissue 1 (t_1).

In this study, several different materials for Tissue 1 and Tissue 2 are investigated. While emphasis is given to measurements conducted with actual biological tissues, we also examine data obtained with other materials in order to achieve a more thorough understanding of the effect of material contribution to the dielectric properties. Thus, for simplicity, "Tissue 1" and "Tissue 2" are used to represent the layers regardless of whether they are actual tissues or other materials.

B. Materials and Measurements

Tissues and materials used in the experiment are selected so as to maximize the range of tissue properties and dielectric contrasts involved in the measurement scenarios.

A summary of the measurement scenarios is provided in Table 1. The first three scenarios (S1, S2, and S3) involve material combinations that are not composed fully, or at all, of biological tissues; whereas the final two scenarios (S4 and S5) involve only biological tissues.

TABLE 1. SUMMARY OF THE MEASUREMENT SCENARIOS.

Scenario	Tissue 1 (Liquid)	Tissue 2 (Solid)
S1	Deionized Water	Acrylic
S2	Duck Fat	Phantom
S3	Physiological Saline	Phantom
S4	Duck Fat	Porcine Muscle
S5	Duck Fat	Porcine Fat

The materials involved in these measurements are: deionized water, physiological (0.9%) saline, acrylic, a rubber-based tissue-mimicking phantom, porcine muscle, porcine fat, and duck fat.

The porcine tissues are fresh excised samples that have never been frozen, and no additional tissue processing is performed except to slice (using a scalpel) the tissue samples into thick slabs for use in the experiment. Whereas the porcine fat was not processed, the duck fat was refined to remove impurities. As a result, these two types of fat have significantly different dielectric properties.

The tissue-mimicking phantom is based on those developed in [25], and has a stable, solid structure. In particular, the phantom is composed of polyurethane, carbon black and graphite. First, the polyurethane is mixed (from part A and part B polyurethane components), then the carbon black and graphite powders are added [25]. The mixture is transferred to a mold in which the phantom is allowed to set prior to usage.

Measurements across all scenarios were performed at room temperature (22℃) in a climate-controlled room. Both room temperature and the temperature of each sample was recorded at each measurement instance, and verified to be stable. The Hanna Checktemp1 EN13485 steel probe thermometer was used for measuring room temperature and the sample temperature of liquids; while the Precision Gold Infrared Thermometer N85FR was used for tissue and phantom samples.

The mean measured relative permittivity and conductivity for the biological tissues are plotted in Figures 3 and 4, respectively. The mean dielectric properties are obtained across ten measurements conducted on each tissue type. The standard deviation of the measurements, for both relative permittivity and conductivity, are noted in the captions of Figures 3 and 4.

For the remaining non-biological materials involved in the experimental design, the mean relative permittivity obtained over 10 measurements is 79, 2.25, 376, and 76, at 300 MHz, for deionized water, acrylic, phantom, and physiological saline, respectively. At 8.5 GHz, the relative permittivity for the acrylic remains constant. For water,

phantom, and saline, the relative permittivity at 8.5 GHz drops to 66, 58, and 64, respectively. In all cases, the standard deviation for these measurements is within the measurement uncertainty of the dielectric measurement system.

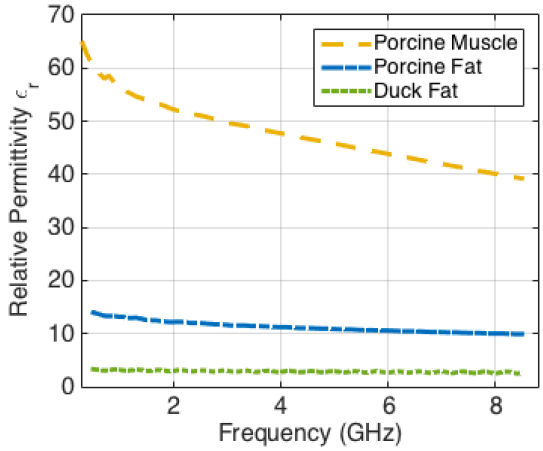

Figure 3. Relative permittivity (ε_r) for the three tissues used in the experiment: porcine muscle (orange, dashed line), porcine fat (blue, dashed-dotted line), and duck fat (green, dotted line). There is a high contrast in the relative permittivity of muscle to either fat tissue, and a lower contrast between the two types of fat. For these measurements, the standard deviation for porcine muscle is 3.7 at 300 MHz and 2.7 at 8.5 GHz, decreasing monotonically across the frequency range. Similarly, the standard deviation for porcine fat is 2.5 and 1.6, respectively, and for duck fat is 0.007 and 0.005, respectively, at the lower and upper frequency limits.

Using these materials, we can therefore vary the magnitude and contrast of Tissue 1 and Tissue 2 across measurement scenarios. For S1, the contrast in relative permittivity is high, at approximately 35:1 at 300 MHz, decreasing to 29:1 at 8.5 GHz. The contrast is slightly lower but still high for S2, at 27:1 for 300 MHz and 22:1 for 8.5 GHz. Uniquely, S3 has a moderate contrast (5:1) at low frequencies, but due to the dispersive properties of the phantom and saline, it has low contrast (1.1:1) at high frequencies. Next, S4 has also moderate contrast, varying from 18:1 at 300 MHz to 15:1 at 8.5 GHz. Lastly, S5 is the lowest contrast scenario at the lower frequencies, with 4.3:1 at the lower frequency limit and 3.9:1 at the upper frequency limit.

For each scenario listed in Table 1, one set of bulk tissue samples is obtained, i.e., the two constituent materials remain the same across all measurements within a scenario, while the thickness of Tissue 1 is varied to obtain different bulk tissue samples. We note that for all scenarios, the increments in measured thicknesses t_1 over a given measurement set are not evenly spaced, as movement of the probe cannot be controlled to sub-mm precision with the current set-up. This, however, does not present a problem as the magnitude of the thickness is easily and precisely measured post-moving of the probe, and a good resolution of distances is obtained. The thickness values are concentrated over distances where the change in permittivity is highest (this range of distances varies based on material properties).

Each set of measurements is repeated 15 times to ensure repeatability; however, the thicknesses of Tissue 1 are not exactly the same in each set (for the reasons discussed in the previous paragraph). Only one set of measurements is used in the analysis – that which has the largest number of points of thickness of Tissue 1. This is important as a higher number of points leads to curves that have higher resolution of information, and this is key when characterizing curves with sharp variations in the dependent variable.

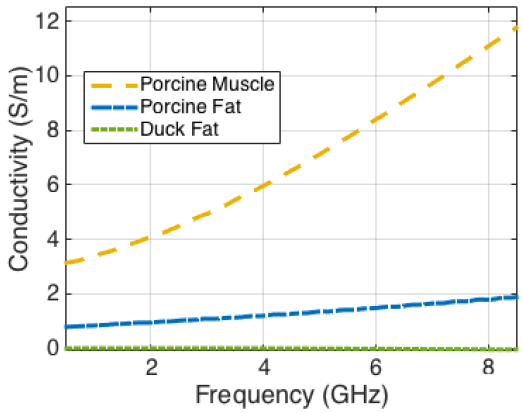

Figure 4. Conductivity for the three tissues used in the experiment: porcine muscle (orange, dashed line), porcine fat (blue, dashed-dotted line), and duck fat (green, dotted line). For these measurements, the standard deviation for porcine muscle is 0.02 at 300 MHz and 0.96 at 8.5 GHz, increasing monotonically across the frequency range. Similarly, the standard deviation for porcine fat is 0.27 and 0.68, respectively, and for duck fat is 0.005 and 0.005, respectively, at the lower and upper frequency limits.

C. *Histology Region*

Histological analysis is conducted on tissue samples in order to determine the types and distributions of tissues present within a bulk tissue sample. This process typically includes preservation of the tissue sample, embedding the sample in wax, then slicing it thinly, staining the slices, and digitally imaging and marking the cells.

For dielectric studies, the Histology Region is defined as the volume within a tissue sample that is subjected to histological analysis. Performing histological analysis on the entire volume of a sample is not necessary for dielectric studies, as the dielectric probe has a limited measurement volume.

The Histology Region is given by the histology depth (d_h) and the histology radius (r_h). Together, these two parameters define a cylindrical volume. The tissues occupying this volume contribute to the dielectric measurement. Outside of this volume, tissues do not contribute to the dielectric measurement. The size of the Histology Region depends on the composition of tissues within the sample, namely, the magnitude of the dielectric properties of the constituent tissues [26].

In this work, the sample heterogeneities are restricted to the longitudinal (depth) direction from the probe tip, and all samples are homogeneous in the radial direction to well beyond the extent of the histology radius. Therefore, this

study focuses on the histology depth. We note that both Tissue 1 and Tissue 2 are sufficiently large that reflections from the radial edges are not seen in dielectric measurements.

The histology depth is determined based on the technique suggested for quantifying the sensing depth of the dielectric probe in [27]. In this way, the dielectric probe is positioned in the tank in contact with Tissue 2, surrounded by the background liquid of Tissue 1. Then, the probe is moved away vertically in small increments until the presence of Tissue 2 is no longer detectable in the measured dielectric properties. In [27], a 10% threshold was used to define the limit of 'detectable', i.e., Tissue 2 is detectable if the presence of Tissue 2 induces a change of more than 10% in the measurement, from the properties of the background liquid (Tissue 1). Here, however, we define the histology depth as the depth at which Tissue 2 ceases to contribute to the measured dielectric properties, within the uncertainty of the measurement.

The measurement set-up with the tank, as described above in Section IIA, results in heterogeneous tissue samples as shown in Figure 5, with the histology depth marked. From the diagram, it is evident that the measurements are performed on samples composed of bilayered material structures. This type of investigation of bulk heterogeneous samples that are composed of homogeneous layers has often been a test scenario in the field of dielectric spectroscopy [17], [28]-[30], and is useful in a wide range of studies including to quantify the sensitivity or specificity of the dielectric probe [28] and to quantify the material properties of the individual layers based on the reflection coefficient measurements [29].

From the diagram in Figure 5, it is clear that the thickness of Tissue 2 that is within the histology depth may be smaller than the actual thickness of Tissue 2. The thickness of Tissue 2 that lies within the histology depth is given by t_2. The thicknesses of the two tissues within the histology depth occupy this depth fully, i.e., $t_1 + t_2 = d_h$.

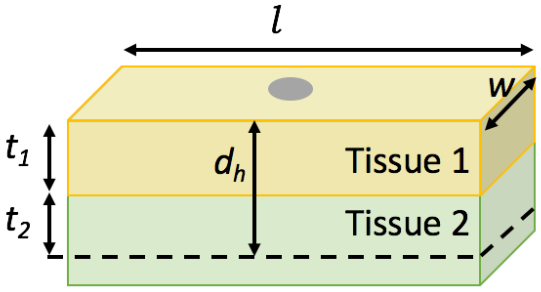

Figure 5. Diagram of a heterogeneous tissue sample, composed of a stack of two tissues: Tissue 1 (yellow) and Tissue 2 (green). The sample width (w) and length (l) are marked, along with the histology depth (d_h). The thickness of Tissue 1 (t_1) and the thickness of Tissue 2 that is within the histology depth (t_2) are also shown. The grey oval indicates the location of the dielectric probe.

In Table 2, the measured histology depths are provided for each heterogeneous sample scenario, at both the lower and upper frequency limits. For all scenarios, the histology depth decreases with increasing frequency. The percent difference between the histology depth at 8.5 GHz and the histology depth at 300 MHz is also provided in the table. The largest absolute change with frequency occurs for S3, where the histology depth decreases by 0.63 mm from 300 MHz to 8.5 GHz. However, for the two scenarios that involve exclusively biological tissues (as opposed to phantoms), i.e., S4 and S5, the histology depth decreases by less than 2% with increasing frequency. As a result, the histology depth can likely be assumed constant across frequency for these scenarios. By taking the average histology depth across frequency and applying it to all frequencies, the error in d_h is less than 0.48% for S4 (fat and muscle) and less than 0.81% for S5 (porcine fat and duck fat). This magnitude of error is negligible, i.e., within the error anticipated by measurement uncertainty.

TABLE 2. HISTOLOGY DEPTH (d_h) FOR EACH HETEROGENEOUS SCENARIO, MEASURED AT 300 MHZ AND 8.5 GHZ. THE PERCENT DIFFERENCE IN THE HISTOLOGY DEPTH AT 8.5 GHZ, RELATIVE TO 300 MHZ, IS ALSO SHOWN.

Scenario	300 MHz	8.5 GHz	% Difference
S1	1.598 mm	1.007 mm	37
S2	2.962 mm	2.527 mm	15
S3	2.230 mm	1.602 mm	28
S4	2.776 mm	2.750 mm	1.0
S5	3.646 mm	3.588 mm	1.6

III. TISSUE CONTRIBUTION TO DIELECTRIC PROPERTIES

In order to attribute dielectric measurement data to heterogeneous tissues, it must be clear which tissues have contributed to the dielectric data and in which proportions. In this work, we examine the two ways that tissues may be characterized as contributing to measured dielectric properties: *i*) based on the contribution of the dielectric properties of each individual tissue to the bulk dielectric properties, and *ii*) based on the volume that each individual tissue occupies within the bulk tissue sample.

It has been typical to state [9], [10], for example, that a bulk tissue sample is composed of 75% fat tissue and 25% glandular tissue, and thus the measured dielectric properties are proportionally resultant from that tissue composition. However, recent studies [16], [17], have suggested that there is not a linear proportionality of contribution, specifically, tissues closer to the probe tip contribute to the dielectric measurement more than tissues further from the probe tip. This finding suggests that the contribution of tissues to the dielectric data is not equal to the proportion of volume occupied by those tissues in the Histology Region.

In this section, the calculation for dielectric contribution (*i*) is presented first, followed by that of the volume contribution (*ii*). Then, in Section IV, we determine these contributions for each of the measurement scenarios and compare them to investigate the relationship between them.

A. Dielectric Contribution

The measured dielectric properties of a heterogeneous tissue sample, as shown in Figure 5, are a result of the dielectric properties of the materials within the Histology Region. The measured dielectric data, $\varepsilon_{r_{meas}}$, for a fixed

sample composition, can be attributed to a combination of the dielectric properties of Tissue 1 and Tissue 2 as follows:

$$\varepsilon_{r_{meas}} = w_{m,T1} * \varepsilon_{r_1} + w_{m,T2} * \varepsilon_{r_2}, \quad (1)$$

where ε_{r_1} is the relative permittivity of Tissue 1; ε_{r_2} is the relative permittivity of Tissue 2; $w_{m,T1}$ is the weight of the contribution of the dielectric properties of Tissue 1, and $w_{m,T2}$ the weight of the properties of Tissue 2, to the measured dielectric properties of the bulk sample. Since there are only two materials present in the vicinity of the probe, their combined contribution must match the total contribution, i.e.,

$$w_{m,T1} + w_{m,T2} = 1. \quad (2)$$

Combining equations (1) and (2), the weights can be solved for directly using:

$$w_{m,T1} = \frac{\varepsilon_{r_{meas}} - \varepsilon_{r_2}}{\varepsilon_{r_1} - \varepsilon_{r_2}}, \quad (3)$$

and

$$w_{m,T2} = \frac{\varepsilon_{r_1} - \varepsilon_{r_{meas}}}{\varepsilon_{r_1} - \varepsilon_{r_2}}. \quad (4)$$

When Tissue 1 is sufficiently thick that Tissue 2 no longer influences the measured dielectric data, then $w_{m,T2}$ = 0, and $\varepsilon_{r_{meas}} = \varepsilon_{r_1}$. Similarly, when the probe is in direct contact with Tissue 2 (i.e., at t_1 = 0 mm), then $w_{m,T1}$ = 0, and $\varepsilon_{r_{meas}} = \varepsilon_{r_2}$.

It is important to note that the weight of contribution of each tissue to the dielectric properties is also dependent on the heterogeneous structure of the tissue sample, as the topmost tissue has a dominant impact on the measured properties [17]. Therefore, while the measured relative permittivity is a linear combination of each individual tissue's relative permittivity for any given sample, the specific linear combination changes based on the sample composition (in this case, based on the thickness of Tissue 1, t_1). In other words, these equations do not assume or imply that $\varepsilon_{r_{meas}}$ is linearly related to t_1.

B. Sample Volume Contribution

The measured dielectric properties are a result of the tissues present in the bulk tissue sample and the relative distributions and proportions of these tissues. In this section, we look at the proportion of the bulk tissue sample volume that is occupied by each tissue (regardless of distribution). The volume occupied by each tissue is a known fixed value and is independent of whether or not the tissues at different depths contribute to the dielectric measurement proportionally.

The volume of the bulk tissue sample that is occupied by Tissue 1 is given by:

$$v_1 = l * w * t_1, \quad (5)$$

where the dimensions are as indicated in Figure 5. Similarly, the volume of the bulk tissue sample that is occupied by Tissue 2 is:

$$v_2 = l * w * t_2. \quad (6)$$

The total volume of the bulk heterogeneous sample is given by:

$$v_{tot} = v_1 + v_2 = l * w * (t_1 + t_2). \quad (7)$$

The weight of volume occupied by each tissue is calculated as the ratio of that tissue's volume to the total sample volume. By using this ratio, and combining equations (5), (6), and (7), we obtain:

$$w_{v,T1} = \frac{v_1}{v_{tot}} = \frac{l*w*t_1}{l*w*(t_1+t_2)} = \frac{t_1}{(t_1+t_2)}, \quad (8)$$

$$w_{v,T2} = \frac{v_2}{v_{tot}} = \frac{l*w*t_2}{l*w*(t_1+t_2)} = \frac{t_2}{(t_1+t_2)}, \quad (9)$$

where $w_{v,T1}$ and $w_{v,T2}$ are the weights of the volume-wise contributions of Tissue 1 and Tissue 2, respectively, to the total sample volume. From equation (9), it is evident that each of the weights is linearly dependent on t_1, for example:

$$w_{v,T2} = \frac{t_2}{(t_1+t_2)} = 1 + \left(\frac{1}{t_1}\right) t_2, \quad (10)$$

and similarly for $w_{v,T1}$.

IV. Measurement Results

In this section, the experimental results are presented. First, examples of dielectric data collected with the measurement set-up are plotted for a large range of t_1 values. Then, the weights of contribution of Tissue 1 and Tissue 2 to the measured dielectric properties are calculated, along with the weights of volume occupied for each tissue.

Throughout, the results focus on the two scenarios that exclusively involve biological tissues (S4 and S5). Further, S1, with acrylic in water, is also discussed in detail because it represents a very highly controlled scenario: the acrylic has no elasticity, and the dielectric properties remain stable over time and temperature. Therefore, it provides a useful test scenario.

A. Measured Data

In this section, the collected data from two example scenarios are presented. Data from the other scenarios follows similar trends. First, the relative permittivity and conductivity of S1, acrylic and water, are plotted in Figures 6 and 7, respectively. This measurement provides an example of a high contrast scenario.

Next, the relative permittivity for S5, duck fat and porcine fat, is plotted in Figure 8, demonstrating a low contrast scenario. For both high and low contrast scenarios, the measurement trends are the same. When t_1 = 0, the measured permittivity is equal to that of Tissue 2 exclusively, and when the probe is far from Tissue 2, i.e., t_1 is sufficiently large, the measured permittivity is equal to that of Tissue 1 exclusively. As t_1 increases from 0 mm (the point at which the probe is in contact with Tissue 2), all permittivity values between those of Tissue 1 and Tissue 2 may be obtained.

B. Calculation of Weights

Next, we calculate the weights of contribution to the dielectric data, $w_{m,T1}$ and $w_{m,T2}$ as in equations (3) and (4), and the weights of volume occupied, $w_{v,T1}$ and $w_{v,T2}$ as in equations (8) and (9), across all t_1 in a given scenario, and plot them side-by-side for ease in comparison.

The weights for Tissue 1 of S4 (porcine muscle and duck fat) are plotted in Figure 9. This data is obtained at 300 MHz; however, as noted in Section IIC, the Histology Region, and thus the weights of volume occupied, are quite constant over frequency for this scenario. Similarly, the

weights for Tissue 2 of S4 are plotted in Figure 10. As expected, the weights for Tissue 2, are equal to one minus the weights for Tissue 1, thus the curves in Figure 10 have the inverse trend relative to those of Figure 9. From Figures 9 and 10, it is clear that the weights of volume occupied ($w_{v,T1}$ and $w_{v,T2}$) are linearly dependent on t_1, as known from equations (7)-(9), up to the point where $\varepsilon_{r_{meas}} = \varepsilon_{r_1}$. Further, the weights of contribution to the dielectric data ($w_{m,T1}$ and $w_{m,T2}$), are not linear with respect to t_1, instead appearing to have an exponential trend.

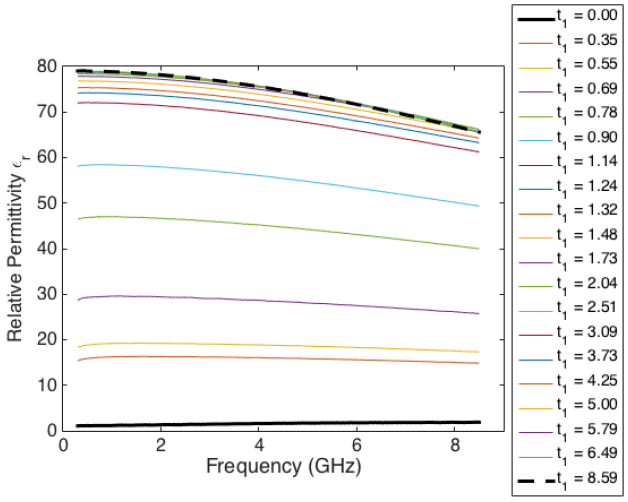

Figure 6. Measured relative permittivity for heterogeneous samples composed of varying thicknesses of deionized water as Tissue 1 and acrylic as Tissue 2 (S1). In this plot, each trace is a unique value for t_1. When $t_1 = 0$ mm, the measured relative permittivity is equal to that of Tissue 2 exclusively; when $t_1 = 8.59$ mm, the measured relative permittivity is equal to that of Tissue 1 exclusively. The magnitude of the relative permittivity decreases monotonically as t_1 increases. The units of t_1 are mm. The standard deviation of each trace is within the measurement uncertainty.

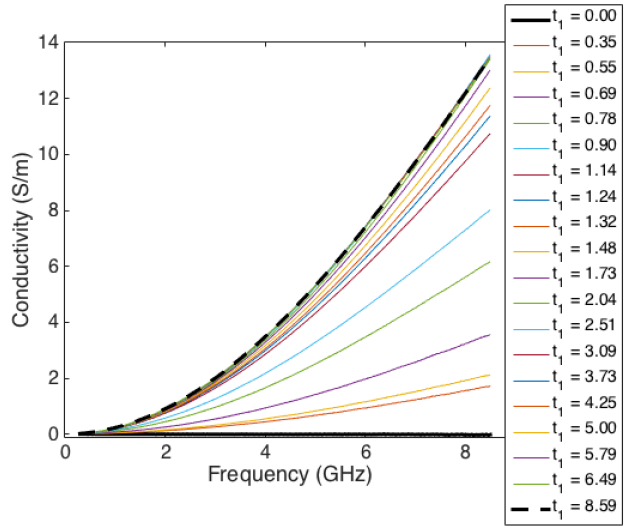

Figure 7. Measured conductivity for heterogeneous samples composed of varying thicknesses of deionized water as Tissue 1 and acrylic as Tissue 2 (S1). In this plot, each trace corresponds to a unique value for t_1. When $t_1 = 0$ mm, the measured conductivity is equal to that of Tissue 2 exclusively; when $t_1 = 8.59$ mm, the measured conductivity is equal to that of Tissue 1 exclusively. The magnitude of the conductivity increases monotonically as t_1 increases. The units of t_1 are mm. The standard deviation of each trace is within the measurement uncertainty.

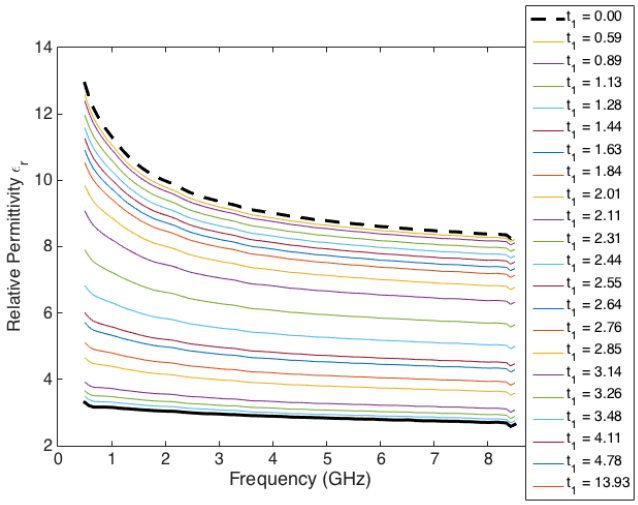

Figure 8. Measured relative permittivity for heterogeneous samples composed of varying thicknesses of duck fat as Tissue 1 and porcine fat as Tissue 2 (S5). In this plot, each trace corresponds to a unique value for t_1. When $t_1 = 0$ mm, the measured relative permittivity is equal to that of Tissue 2 exclusively; when $t_1 = 13.93$ mm, the measured relative permittivity is equal to that of Tissue 1 exclusively. As with the materials in Figure 6, the magnitude of the relative permittivity decreases monotonically as t_1 increases. The units of t_1 are mm. The maximum standard deviation (across all traces) is 2.5.

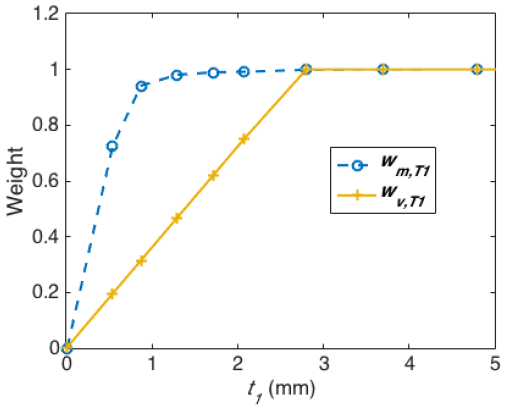

Figure 9. Weights for Tissue 1 in S4 (from measurement at 300 MHz): weight of dielectric properties to total measured dielectric data, $w_{m,T1}$ (blue, dashed line with circles), and weight of volume occupied of Tissue 1 relative to total sample volume, $w_{v,T1}$ (orange, solid line with '+'s).

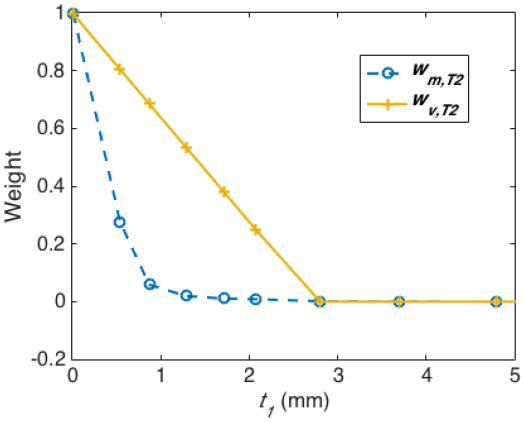

Figure 10. Weights for Tissue 2 in S4 (from measurement at 300 MHz): weight of dielectric properties to total measured dielectric data, $w_{m,T2}$ (blue, dashed line with circles), and weight of volume occupied of Tissue 2 relative to total sample volume, $w_{v,T2}$ (orange, solid line with '+'s).

Next, in the same way as above, the weights for Tissue 1 of S5 (porcine fat and duck fat) are plotted in Figure 11. As the weights for Tissue 2 can be inferred from Figure 11, they are not plotted. As with S4, and as expected, the weights of volume occupied are linearly dependent on t_1. However, the weights of contribution to the dielectric data follow an s-shaped curve.

For the remaining three scenarios, the curves of weights of volume occupied and weights of contribution to the dielectric data follow similar trends either to those shown in Figure 9 or in Figure 11. Importantly, if the histology depth is assumed constant, then the weights of volume occupied are the same regardless of which tissue types are involved, while the weights of contribution to the dielectric data are independent of the histology depth.

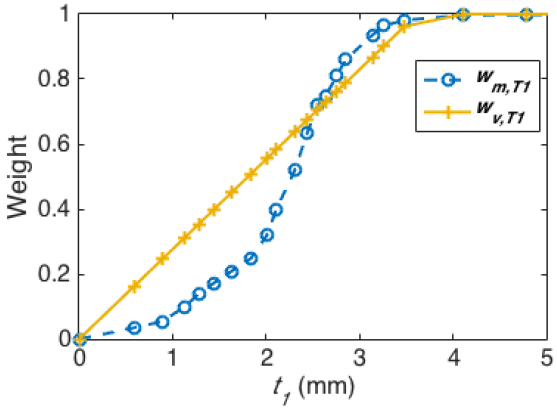

Figure 11. Weights for Tissue 1 in S5 (from measurement at 300 MHz): weight of dielectric properties to total measured dielectric data, $w_{m,T1}$ (blue, dashed line with circles), and weight of volume occupied of Tissue 1 relative to total sample volume, $w_{v,T1}$ (orange, solid line with '+'s).

Next, the difference between the two types of weights is investigated. This difference is examined since, historically, studies have assumed that there is no difference between these values. Therefore, assuming that the two weight values are equal could be a factor that adds error to dielectric measurements of heterogeneous tissues.

The difference in weights for both Tissue 1 and Tissue 2 is plotted for S4 in Figure 12 and for S5 in Figure 13. In Figure 12, for each t_1, the magnitude of the difference between the two weights for Tissue 1 is equal to the difference between the weights for Tissue 2. The maximum difference between the two types of weights is 0.63, at t_1 = 0.87 mm. If these weights were assumed to be equal in a dielectric study, then an error of 0.63 between them is is significant, as it indicates that the majority tissue type that contributes to the dielectric measurement is not correctly identified. In Figure 13, the maximum error between the weights for S5 is 0.26, and occurs at t_1 = 1.84 mm. The difference in weights follow similar trends for the other scenarios.

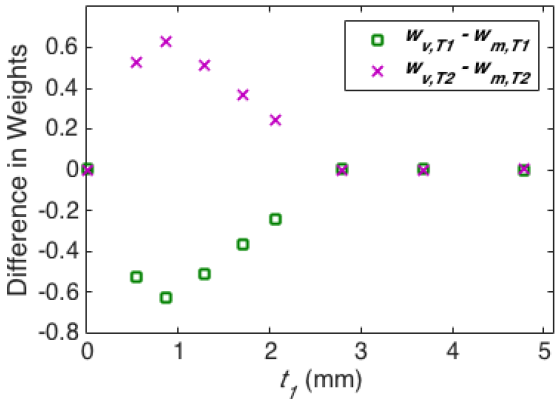

Figure 12. Difference in weights versus t_1, for S4 (from measurement at 300 MHz). The magnitude of the difference in weights is equal at each t_1 for Tissue 1 and Tissue 2.

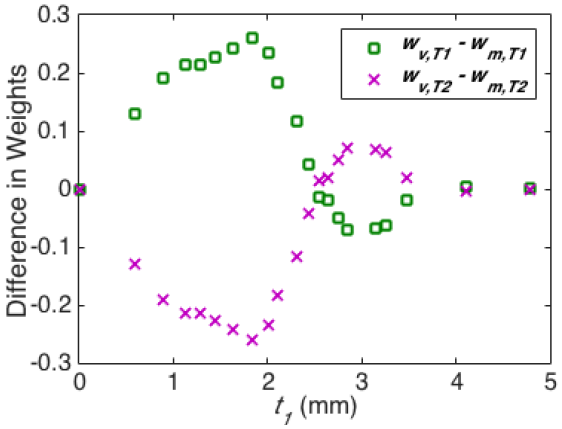

Figure 13. Difference in weights versus t_1, for S5 (from measurement at 300 MHz). The magnitude of the difference in weights is equal at each t_1 for Tissue 1 and Tissue 2.

From these results, it is clear that the weights for dielectric contribution do not correspond well with the volume occupied. In all scenarios, there is a significant mismatch between the percent of volume occupied by a tissue and the percent that that tissue contributes to the measured dielectric properties. There is no linear relation between the volume occupied of a tissue and the dielectric contribution of that tissue to the measured data. Further, making the assumption that these are equivalent can lead to significant errors of up to tens of percentage points, depending on the measurement scenario. In the next section, we provide a model that enables a good match between the volume occupied and the contribution to the dielectric data.

V. Modelling

In this section, we model the relationship between the volume occupied by the tissues in the bulk sample and their contribution to the dielectric measurement of that sample. More specifically, we identify an equation that describes the contribution of the tissues to the dielectric data for all measurement scenarios, and link this to the volume of the tissues within the sample.

The weights of contribution to dielectric properties, $w_{m,T1}$ and $w_{m,T2}$, appear in Figure 9 to follow a bounded exponential curve, while in Figure 12 they follow an s-shaped curve. Thus we have identified the logistic function as being a good candidate to fit both of these data sets, as it provides the combination between the exponential and bounded exponential curve characteristics of the s-shaped curve.

The weights of contribution of Tissue 1 and Tissue 2 to the dielectric data depend on the thickness of Tissue 1 (t_1), i.e., they depend on the bulk sample composition. Thus, the model that represents these weights must also be dependent on t_1. The models for the weights are given by:

$$w_{m,T1} = \frac{1}{1+e^{-\alpha(t_1-\beta)}}, \quad (11)$$

and

$$w_{m,T2} = 1 - \left(\frac{1}{1+e^{-\alpha(t_1-\beta)}}\right), \quad (12)$$

where α gives the steepness of the curve and β defines the midpoint of the s-shape. For both models, the bound, i.e., the numerator of the fraction, is taken to be 1 since this is physically the maximum value that either of the weights can attain (each tissue can only contribute up to 100% of the dielectric properties). Finally, the relative permittivity can be calculated using this model as:

$$\varepsilon_{r,calc} = w_{m,T1} * \varepsilon_{r_1} + w_{m,T2} * \varepsilon_{r_2}, \quad (13)$$

in a similar manner to that shown in equation (1).

Using equations (11) and (12), models are fitted to the weights for each scenario at both the lowest and highest measured frequencies. The data is fitted using nonlinear least squares to minimize the error between the measured data and the model.

As an example, the weights $w_{m,T2}$ for S4 are plotted in Figure 14 along with the best fit model. In this case, the logistic provides a high quality fit with a mean error of only 0.01. The best fit parameters for $w_{m,T1}$ are the same as those for $w_{m,T2}$, however the shape of the curve is inverted.

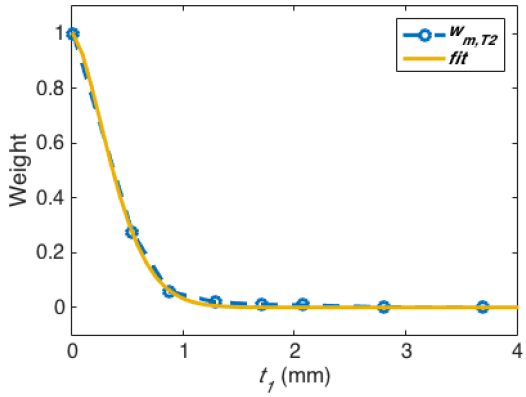

Figure 14. Weights of Tissue 2 contribution to measured dielectric data (blue, dashed line with circles) and fitted model (orange, solid line) for S4 (muscle and fat).

Next, Figure 15 summarizes the resulting models, while Table 3 provides a summary of the obtained best fit parameters α and β, and fit error, for each scenario. In all scenarios, the fit error is low. Further, from Figure 15, it is evident that the α and β parameters vary widely across measurement scenarios, as in some cases the curve for weight of contribution of Tissue 1 to the dielectric measurement increases quickly with increasing t_1, while in other cases the increase is more gradual. It is also found that for some measurement scenarios, namely S1 (acrylic and water) and S2 (duck fat and phantom), there is very little dependence of the weights on frequency. For S4 (muscle and duck fat) and S5 (porcine fat and duck fat), the weights for each t_1 change only slightly with frequency. In S3 (saline and phantom), however, there is a significant change with frequency. As discussed in Section IIB, the material properties in S3 are dispersive in such a way that the material that has a higher magnitude permittivity at 300 MHz is the one that has a lower permittivity at 8.5 GHz. In other words, a cross-over in the dielectric properties occurs partway through the frequency range, significantly altering the dielectric contrast between the materials cross the band. For this reason, the contribution of Tissue 1 to the dielectric measurement changes with frequency more than in any other scenario. This characteristic of the materials involved in S3 demonstrates that it cannot always be assumed that the weights will be constant with frequency.

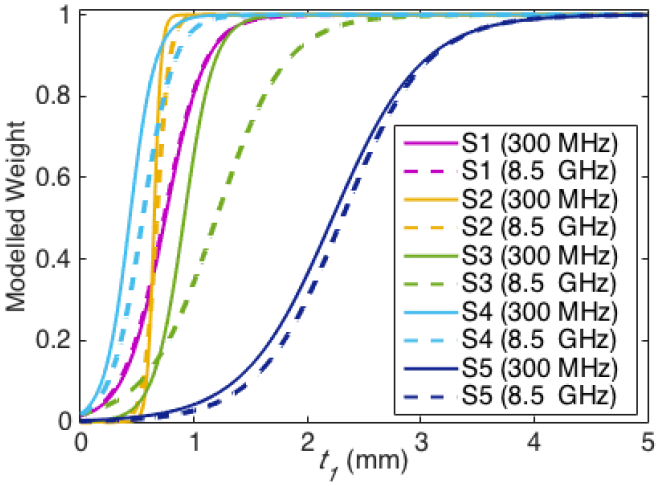

Figure 15. Model weights for Tissue 1 for all scenarios, shown for the lowest frequency of measurement 300 MHz and the highest frequency 8.5 GHz. It is evident that the contribution of Tissue 1 to the measured dielectric properties depends on the thickness of Tissue 1, t_1, and further, is highly dependent upon the material properties involved in the various scenarios.

TABLE 3. BEST FIT PARAMETERS AND MEAN FIT ERROR (CALCULATED BETWEEN MEASURED WEIGHTS AND FITTED MODEL) FOR ALL SCENARIOS.

Scenario	f	α	β	fit error
S1 (Water/Acrylic)	300 MHz	5.64	0.75	0.016
	8.5 GHz	5.57	0.74	0.014
S2 (Fat/Phantom)	300 MHz	32.5	0.65	0.014
	8.5 GHz	18.2	0.67	0.010
S3 (Saline/Phantom)	300 MHz	7.53	0.91	0.014
	8.5 GHz	3.29	1.20	0.028
S4 (Fat/Muscle)	300 MHz	8.90	0.43	0.011
	8.5 GHz	7.27	0.55	0.009
S5 (Fat/Fat)	300 MHz	2.55	2.22	0.023
	8.5 GHz	2.71	2.31	0.018

VI. Discussion

We next examine the point at which both Tissue 1 and Tissue 2 contribute equally to the dielectric measurement. From the literature [17], and confirmed in Section III, we know that the tissues do not contribute equally to the dielectric measurement when $t_1 = t_2$, as the layer of material closest to the probe tip dominates the measurement. In Table 4, the thicknesses of Tissue 1 at which equal (50-50) contribution to dielectric properties occurs is listed for all scenarios. For S1, at the point where the tissues contribute equally to the dielectric properties, the thickness of the two tissues are the closest to equal at 300 MHz, with t_1 = 0.75 mm and t_2 = 0.85 mm. For the same frequency with S2, S3, and S4, the thickness of Tissue 1 is 1.5 to 6 times smaller than that of Tissue 2 when the tissues contribute equally to the dielectric properties. However, for S5, the thickness of Tissue 1 is larger than that of Tissue 2 when they contribute equally to the dielectric data, likely due to the low contrast and similar properties between the two tissues.

Significantly, the thickness of Tissue 1 when the 50-50 contribution occurs varies widely across measurement scenarios. For example, when the t_1 value is large enough to reach the 50-50 contribution point in S5, all of the other measurement scenarios are at 100-0 contribution (i.e., Tissue 1 is the only tissue that contributes to the dielectric properties, and the dielectric properties of Tissue 2 do not impact the measurement result). This finding indicates that it is not reasonable to assume a single logistic curve with the same parameters for all measurement scenarios, as this would introduce large errors in assigning the dielectric properties to the tissues that have contributed to them.

TABLE 4. THICKNESS OF TISSUE 1 (t_1) AT WHICH A 50-50 CONTRIBUTION OF TISSUES 1 AND 2 TO THE DIELECTRIC PROPERTIES OCCURS, AND THE CORRESPONDING THICKNESS OF TISSUE 2 (t_2) AT THAT POINT.

Scenario	f = 300 MHz		f = 8.5 GHz	
	t_1 (mm)	t_2 (mm)	t_1 (mm)	t_2 (mm)
S1	0.75	0.85	0.74	0.27
S2	0.65	2.31	0.67	1.86
S3	0.91	1.32	1.20	0.40
S4	0.43	2.35	0.54	2.21
S5	2.22	1.43	2.31	1.28

In order to verify the accuracy of using the modelled weights to calculate the relative permittivity, we apply equation (13) with the model weights and obtain $\varepsilon_{r,calc}$. This calculated permittivity is then compared to the measured relative permittivity (1). The results are shown in Table 5. For all scenarios and frequencies, the error between the calculated and measured relative permittivity is at or below the measurement uncertainty. This result confirms that the model is an accurate representation of the measured dielectric data.

TABLE 5. PERCENTAGE ERROR BETWEEN $\varepsilon_{r,calc}$ AND $\varepsilon_{r,meas}$, FOR EACH MEASUREMENT SCENARIO AND FREQUENCY.

Scenario	300 MHz	8.5 GHz
S1 (Water/Acrylic)	1.0%	0.8%
S2 (Fat/Phantom)	2.6%	1.2%
S3 (Saline/Phantom)	2.0%	0.3%
S4 (Fat/Muscle)	2.6%	2.0%
S5 (Fat/Fat)	2.7%	1.8%

Therefore, using these models, one can predict what the measured permittivity will be based on knowledge of t_1, or predict t_1 based on the measured permittivity. However, the prediction is only accurate if the types of materials involved in the tissue sample is known, allowing us to determine the model parameters α and β. For this reason, this simplified model is only the first step towards the development of a comprehensive model, which will relate d_h, α, and β to factors that influence the ability of the coaxial probe to measure heterogeneities at different depths, namely, the attenuation of the electromagnetic signal within the tissues, the noise floor of the measurement system, and the power of the transmitted electromagnetic signal. Thus, these results may be treated as a stepping stone towards the development of more complex models that map the relationship between heterogeneous tissues (both radially and longitudinally) and measured dielectric properties. This work has provided a much needed deeper understanding of how longitudinal heterogeneities within the histology depth impact the dielectric measurement, and quantified the nonlinear relationship between these variables.

VII. Conclusion

In this work, the impact of tissue heterogeneities on the dielectric measurement of biological tissues was investigated. Specifically, measurements were performed on heterogeneous samples composed of layers of two materials types, with varying thickness of the top material. For materials including standard liquids, phantoms, and muscle and fat tissue, the weight of the contribution of each tissue to the measured dielectric data was calculated. The relative volume occupied by each tissue, within the bulk sample, was also calculated. These two values were compared, and it was found that the relationship between the volume occupied by the tissue and the contribution of the tissue to the dielectric measurement is nonlinear. Finally, a model was developed that relates the tissue thickness (and thus volume) to the dielectric contribution. This work provides a step towards being able to predict the dielectric measurement based on histology of a heterogeneous tissue sample, and vice versa. This goal is vital to achieving accurate dielectric measurements of heterogeneous tissues, which are strongly needed by the electromagnetic medical device community.

ACKNOWLEDGMENT

The research leading to these results has received funding from the European Research Council under the European Union's Horizon 2020 Programme/ERC Grant Agreement BioElecPro n. 637780, Science Foundation Ireland (SFI) grant number 15/ERCS/3276, and the Natural Sciences and Engineering Research Council of Canada (NSERC). This work has been developed in the framework of COST Action MiMed (TD1301).

REFERENCES

[1] C. Gabriel, S. Gabriel, and E. Corthout, "The dielectric properties of biological tissues: I. Literature survey," *Phys. Med. Biol.*, vol. 41, pp. 2231-2249, 1996.

[2] T. Grzegorczyk, P. M. Meaney, P. A. Kaufman, R. M. diFlorio-Alexander, and K. D. Paulsen, "Fast 3-D Tomographic Microwave Imaging for Breast Cancer Detection," *IEEE Trans. Med. Imag.*, vol. 31, no. 8, pp. 1584-1592, Aug. 2012.

[3] J. Bourqui, J. M. Sill, and E. C. Fear, "A Prototype System for Measuring Microwave Frequency Reflections from the Breast," *International Journal of Biomedical Imaging*, vol. 2012, pp. 1-12, Article ID 851234, 2012.

[4] E. Porter, H. Bahrami, A. Santorelli, B. Gosselin, L. Rusch, M. Popović, "A Wearable Microwave Antenna Array for Time-Domain Breast Tumor Screening," *IEEE Trans. Med. Imag.*, vol. 35, no. 6, pp. 1501-1509, 2016.

[5] T. Sherertz and C. J. Diederich, "Hyperthermia in Locally Recurrent Breast Cancer," in Radiation Therapy Techniques and Treatment Planning for Breast Cancer, Springer International Publishing, Switzerland, 2016, Ch. 9, pp. 145-158.

[6] P. T. Nguyen, A. Abbosh, and S. Crozier, "Microwave Hyperthermia for Breast Cancer Treatment Using Electromagnetic and Thermal Focusing Tested on Realistic Breast Models and Antenna Arrays," IEEE Trans. Antennas Propag., vol. 63, no. 10, pp. 4426-4434, 2015.

[7] W. Zhou, M. Liang, H. Pan, X. Liu, Y. Jiang, Y. Wang, L. Ling, Q. Ding, S. Wang, "Comparison of Ablation Zones among Different Tissues Using 2450-MHz Cooled-Shaft Microwave Antenna: Results in *Ex Vivo* Porcine Models," *PLoS ONE*, vol. 8, no. 8, Article ID: e71873, 2013.

[8] X. Nie, Q. Nan, X. Guo, Z. Tian, "Numerical study of the effect of blood vessel on the microwave ablation shape," *Biomed. Mater. Eng.*, vol. 26, pp. S265-S270, 2015.

[9] M. Lazebnik, L. McCartney, D. Popovic, C. B. Watkins, M. J. Lindstrom, J. Harter, S. Sewall, A. Magliocco, J. H. Booske, M. Okoniewski, and S. C. Hagness, "A large-scale study of the ultrawideband microwave dielectric properties of normal breast tissue obtained from reduction surgeries," *Phys. Med. Biol.*, vol. 52, pp. 2637-2656, 2007.

[10] M. Lazebnik, D. Popovic, L. McCartney, C. B. Watkins, M. J. Lindstrom, J. Harter, S. Sewall, T. Ogilvie, A. Magliocco, T. M. Breslin, W. Temple, D. Mew, J. H. Booske, M. Okoniewski2 and S. C Hagness, "A large-scale study of the ultrawideband microwave dielectric properties of normal, benign and malignant breast tissues obtained from cancer surgeries," *Phys. Med. Biol*., vol. 52, no. 20, pp. 6093-6115, 2007.

[11] T. Sugitani, S. Kubota, S. Kuroki, K. Sogo, K. Arihiro, M. Okada, T. Kadoya, M. Hide, M. Oda, and T. Kikkawa, "Complex permittivities of breast tumor tissues obtained from cancer surgeries," *Appl. Phys. Lett.*, vol. 104, no. 253702, pp. 1-5, 2014.

[12] R. J. Halter, T. Zhou, P. M. Meaney, A. Hartov, R. J. Barth Jr, K. M. Rosenkranz, W. A. Wells, C. A. Kogel, A. Borsic, E. J. Rizzo and K. D. Paulsen, "The correlation of *in vivo* and *ex vivo* tissue dielectric properties to validate electromagnetic breast imaging: initial clinical experience," *Physiol. Meas.*, vol. 30, pp. S121-S136, 2009.

[13] W. T. Joines, Y. Zhang, C. Li, and R. L. Jirtle, "The measured electrical properties of normal and malignant human tissues from 50 to 900 MHz," *Med. Phys.,* vol. 21, pp. 547-550, 1994.

[14] S. S. Chaudhary, R. K. Mishra, A. Swarup, and J. M. Thomas, "Dielectric properties of normal and malignant human breast tissues at radiowave and microwave frequencies," *Indian J. Biochem. Biophys.,* vol. 21 pp. 76–79, 1984.

[15] Keysight Technologies, "85070E Dielectric Probe Kit 200 MHz to 50 GHz Technical Overview," 2015.

[16] P. M. Meaney, A. P. Gregory, N. Epstein, and K. D. Paulsen, "Microwave open-ended coaxial dielectric probe: interpretation of the sensing volume re-visited," *BMC Med. Phys*., vol. 14, no. 3, pp. 1-11, June 2014.

[17] P. M. Meaney, A. P. Gregory, J. Seppala, and T. Lahtinen, "Open-Ended Coaxial Dielectric Probe Effective Penetrative Depth Determination," *IEEE Trans. Microw. Theory Techn.*, vol. 64, no. 3, pp. 915-923, March 2016.

[18] Nephron, Wikimedia Commons, "Very high magnification micrograph of an acinic cell carcinoma," October 2016, [Online] https://commons.wikimedia.org/w/index.php?curid=17150203

[19] L. Abdilla, C. Sammut, and L. Z. Mangion, "Dielectric properties of muscle and liver from 500 MHz – 40 GHz," *Electrom. Biol. Med.*, vol. 32, no. 2, pp. 244-252, 2013.

[20] V. Lopresto, R. Pinto, G. A. Lovisolo, and M. Cavagnaro, "Changes in the dielectric properties of *ex vivo* bovine liver during microwave thermal ablation at 2.45 GHz," *Phys. Med. Biol., vol.* 57, pp. 2309-2327, 2012.

[21] C. Gabriel, and A. Peyman, "Dielectric measurement: error analysis and assessment of uncertainty," *Phys. Med. Biol.*, vol. 51, pp. 6033-6046, 2006.

[22] D. Byrne and I. J. Craddock, "Time-domain Wideband Adaptive Beamforming for Radar Breast Imaging," *IEEE Trans. Antennas Propag.*, vol. 63, no. 4, pp. 1725-1735, 2015.

[23] X. Zeng, A. Fhager, P. Linner, M. Persson, and H. Zirath, "Design and Performance Evaluation of a Time Domain Microwave Imaging System," *Int. J. Microw. Sci. Tech.*, vol. 2013, Article ID 735692, 2013.

[24] A. W. Preece, I. J. Craddock, M. Shere, L. Jones, and H. L. Wintond, "MARIA M4: clinical evaluation of a prototype ultrawideband radar scanner for breast cancer detection," *J. Med. Imag.*, vol. 3., no. 3, Article 033502, 2016.

[25] A. Santorelli, O. Laforest, E. Porter, M. Popović, "Image Classification for a Time-Domain Microwave Radar System: Experiments with Stable Modular Breast Phantoms," in *Proc. 9th European Conference on Antennas and Propagation (EUCAP)*, Lisbon, Portugal, Apr. 12–17, 2015.

[26] E Porter, A. la Gioia, and M. O'Halloran, "Impact of Histology Region Size on Measured Dielectric Properties of Biological Tissues," *Progress in Electromagnetics Symposium (PIERS)*, St. Petersburg, Russia, May 22-25, 2017.

[27] D. M. Hagl, D. Popovic, S. C. Hagness, J. H. Booske, and M. Okoniewski, "Sensing Volume of Open-Ended Coaxial Probes for Dielectric Characterization of Breast Tissue at Microwave Frequencies," *IEEE Trans. Microw. Theory Techn.*, vol. 51, no. 4, pp. 1194-1206, Apr. 2003.

[28] S. Huclova, D. Baumann, M. S. Talary and J. Frohlich, "Sensitivity and specificity analysis of fringing-field dielectric spectroscopy applied to a multi- layer system modelling the human skin," *Phys. Med. Biol.*, vol. 56, pp. 7777-7793, 2011.

[29] G. Chen, K. Li, and Z. Ji, "Bilayered dielectric measurement with an open-ended coaxial probe," *IEEE Trans. Microw. Theory Techn.*, vol. 42, no. 6, pp. 966-971, 1994.

[30] E. Alanen, T. Lahtinen and J. Nuutinen, "Variational formulation of open-ended coaxial line in contact with layered biological medium," *IEEE Trans. Biomed. Eng.*, vol. 45, no. 10, pp. 1241–1248 , 1998.

Emily Porter (S'11, M'15) received the B.Eng., M.Eng., and Ph.D. degrees in electrical engineering from McGill University, Montreal, Canada, in 2009, 2010, and 2015 respectively. Dr. Porter was a recipient of the 2013 IEEE Antennas and Propagation Society Doctoral Research Award for her work on breast health monitoring using a time-domain microwave system. Since 2015, she has been a postdoctoral researcher with the

Translational Medical Device Laboratory at the National University of Ireland Galway. Her current research interests include the measurement of dielectric properties of biological tissues and the development novel technologies for therapeutic and diagnostic applications of electromagnetic waves.

Alessandra La Gioia is a Ph.D. student in the Translational Medical Device Laboratory, funded by European Research Council and led by Dr. Martin O'Halloran, at National University of Ireland, Galway (NUIG). She completed her Bachelor's and Master's degrees in Biomedical Engineering at the University of Bologna (Italy) with first-class honours. Currently, she is investigating techniques for the analysis of the dielectric properties of biological tissues, as a platform for low-cost medical device design.

Adam Santorelli (S'11) is a Postdoctoral Researcher. He completed his B. Eng at in Electrical Engineering in 2010, his M. Eng in Electromagnetics in 2012, and his Ph.D. in 2017, at McGill University in Montreal, Canada. Adam's research interests are focused on biomedical applications with the primary goal of increasing the accessibility to technology in order to improve diagnosis, including the optimization and miniaturization of off-the-shelf components to design and fabricate custom-built low-cost microwave systems. He received the 2nd Place Best Student Paper Award at the 2014 IEEE Sensors Application Symposium.

Martin O'Halloran received a B.Eng. (Hons.) and Ph.D. in Electrical Engineering from the National University of Ireland Galway (NUIG) in 2004 and 2009, respectively. He also holds an MSc. in Clinical Research (2014), also from NUIG. Dr. O'Halloran is the Director of the Translational Medical Device Lab at NUIG, and is Director of Enabling Technologies at BioInnovate (an affiliate of Stanford's BioDesign Programme). He has over 25 national and international awards, including Engineers Ireland Engineer of the Year 2014, and Science Foundation Ireland's EC Researcher of the Year 2016. Dr. O'Halloran's research is funded by Science Foundation Ireland, the Irish Research Council and the European Research Council. His research is focused on patient-centered medical device design and development.